Int. J. Electrochem. Sci., 16 **(2021)** Article ID: 210436, doi: 10.20964/2021.04.61

International Journal of
ELECTROCHEMICAL
SCIENCE
www.electrochemsci.org

Corrosion Behaviour of Welded Steel Bars in Concrete with and without Cracks under Potentiostatic Conditions

Shicai Li, Zuquan Jin[*], *Xiaoying Zhang*

Engineering Research Center of Concrete technology in marine environment, Ministry of Education, Qingdao University of Technology, Qingdao 266033, China
[*]E-mail: jinzuquan@126.com

Received: 15 December 2020 / *Accepted:* 7 February 2021 / *Published:* 28 February 2021

Welding is a simple and effective way to connect steel bars in concrete structures. However, the high temperature during welding can affect the phase composition of the steel bars. In particular, when the welding part is located at the crack, it will be directly affected by corrosion ions, which will destroy the corrosion resistance and the durability of the steel bars. This study aimed to investigate the effects of welding on the corrosion behaviour of steel bars in concrete with and without cracks under potentiostatic acceleration. The corrosion time of the steel bar is shortened 48 h by welding, and the depassivation time of welded corrosion-resistant steel bars was approximately 18 h shorter than that of welded ordinary steel bars. In addition, the depassivation time of the welded steel bars and that of nonwelded bars in concrete was advanced by approximately 15 h and 14 h, respectively, due to cracks. Because the progress of galvanic corrosion has been promoted, the influence is most significant when the type of welded steel bar is LC & CR. For the welded LC & LC types, the corrosion current density was increased by cracks.

Keywords: crack; concrete; welding; potentiostatic acceleration; corrosion behaviour

1. INTRODUCTION

Many RC structures, such as cross-ocean tunnels, sea-crossing bridges, and harbour, are exposed to marine environments containing chloride ions and sulfate ions, which leads to a series of durability problems [1]. Corrosion is one of the critical factors reducing the durability of concrete in marine and other severely corrosive environments. In 2014, the loss caused by corrosion in China was approximately 2,127.8 billion RMB, accounting for 3.34% of the county's GDP [2]. How to eliminate and slow down the corrosion of steel bars is one of the most urgent problems to be solved in practical engineering [3, 4].

Currently, some efficient strategies are being developed to reduce the risk of reinforcement corrosion [5], and include the use of high-performance concrete, protective coatings, corrosion

inhibitors, etc. In addition, using corrosion-resistant steel bars as a method to avoid reinforcement corrosion from the fundamental way has been widely studied. Adding Cr, Ni, Mo, and other alloying elements to obtain corrosion-resistant steel bars can significantly prolong the service life of concrete structures in the ocean and severely corrosive environments [6-8]. Since the cost of stainless steel bars and corrosion-resistant steel bars is 3 to 5 times that of ordinary steel bars, the use of welded steel bars in severely corrosive areas such as ocean splash areas and tidal areas is currently a common choice [9-12]. However, the problem of connecting corrosion-resistant steel bars with ordinary steel bars or corrosion-resistant steel bars will undoubtedly appear in welded steel bars. Some researchers have found that the probability of corrosion at welded joints is high [13-15]. Weld decay, which is severe intergranular corrosion in the heat-affected zone (HAZ), is a common and serious problem encountered during the welding of austenitic stainless steel [16-18]. Some researchers have shown that the chloride threshold value for the initiation of corrosion in nonwelded rebar is approximately 3 to 5 times higher than that in conventional rebar. However, the welding of stainless steel reduced the critical chloride level by 50% [19-21]. Experimental results from Gnanarathinam [22] showed that weldments have high corrosion resistance at room temperature and that the rate of corrosion increases with respect to the temperature and welding time. However, current research has focused on the microstructure and mechanical properties of weldments. Only a few studies on the corrosion of welded steel in concrete have been conducted.

In addition, once steel bars are corroded, the expansion stress generated by the corrosion products will inevitably lead to cracks in the concrete. Cracks can accelerate corrosion by providing a convenient path for the penetration of corrosion substances (water, oxygen, carbon dioxide, chloride, etc.) [23, 24]. If the corrosion process occurs cyclically, the failure of the RC structures cannot be avoided. Therefore, studying the influences of cracks on steel corrosion in concrete is of great significance for the prediction of the durability and service life of marine concrete structures. Numerous experimental and theoretical studies have investigated the influences of cracks on the durability of reinforced concrete by studying chloride penetration [25-27] and steel corrosion in concrete structures [28-30]. Experimental results from Du et al. [31] showed that cracks have a greater influence on reinforced concrete under electrochemical corrosion conditions than under natural exposure conditions. Natural corrosion is two orders of magnitude faster than accelerated corrosion when the crack width is over 0.20 mm. Experimental results from Ji et al. [32]showed that the steel in cracks was activated once transverse cracks occurred in concrete. Additionally, if cracks in concrete are located at the weld joints of the welded steel bars, the rapid intrusion of water and corrosion ions will accelerate damage to the connectivity and durability of the steel bars. However, there is almost no research on the effect of cracks on the corrosion of welded steel bars in concrete.

As mentioned above, cracks and welding can both accelerate reinforcement corrosion. Although many experiments and much research have been carried out, there is still a gap in realizing the relation between welds and cracks and their effect on reinforcement corrosion. Hence, in this study, reinforced concretes with and without cracks were prepared and chloride migration was induced via potentiostatic acceleration. The influence of welding on the corrosion behaviour of steel bars in concrete with and without cracks was studied by electrochemical technology. The results of this study may help to propose

a more reasonable steel connection method and provide a reference for the indicators of cracks at the steel connection.

2. EXPERIMENTS

2.1 Materials

Portland cement P·I.52.5 was used as the binder material. Class I fly ash (FA) and S95 granulated blast furnace slag (GGBS) were used as mineral admixtures. Their chemical compositions are shown in Table 1. River sand (with a fineness modulus of 2.6) was used as the fine aggregate, and crushed granite (with a maximum size of 20 mm) was used as the coarse aggregate.

Table 1. Chemical compositions of cement, fly ash, and GGBS (wt %)

Chemical composition	LOI	SiO_2	Al_2O_3	Fe_2O_3	CaO	SO_3	MgO	K_2O	Na_2O
Cement	0.77	20.87	4.87	3.59	64.49	2.52	2.13	0.65	0.11
FA	0.77	4.09	47.86	35.5	4.52	1.05	0.55	1.18	1.62
GGBS	3.38	33.87	34.59	18.15	0.7	6.5	1.27	0.57	

In this study, two types of steel bars (Q235 low carbon steel and corrosion-resistant steel) with a length of 300 mm and a diameter of 10 mm were used. Corrosion-resistant steel (CR) was alloyed with Cr and Mo and developed by Southeast University [33]. The chemical compositions of the steel bars are shown in Table 2.

Table 2. Chemical compositions of steel bars

Type	Chemical composition								
	Fe	C	Si	Mn	P	S	V	Cr	Mo
CR	Bal.	0.01	0.49	1.49	0.01	0.01	0.06	10.36	1.16
LC	Bal.	0.23	0.52	1.42	0.04	0.03	0.03	-	-

Table 3. Physical properties of steel bars

	Rm (MPa)	*ReL* (MPa)	*Rp* (MPa)	*Lo* (cm)	*Lu* (cm)	Elongation
Nonwelded	678	552	568	20	23.9	19.5%
Welded	655	517	511	20	24.1	20.5%

where *Rm* is the tensile strength, *ReL* is the lower yield strength, *Rp* is the specified nonproportional elongation strength, *Lo* is the original gauge length, and *Lu* is the final gauge length.

To explore the influence of welded steel bars of different welding types on their corrosion resistance, two types of steel bars were welded separately, welded low-carbon steel and low-carbon steel (LC & LC), welded low-carbon steel and corrosion-resistant steel (LC & CR), welded corrosion-resistant steel and corrosion-resistant steel (CR & CR). The physical properties of the welded and nonwelded corrosion-resistant steel obtained by the test are shown in Table 3.

Tensile tests were carried out on the corrosion-resistant reinforcement after welding, and the morphology of the tensile reinforcement is shown in Figure 1. Obviously, the damage point of the welded corrosion-resistant steel bar under tension is not located at the welding joints. As shown in Table 3, the tensile strength after welding is 655 Mpa, indicating that the welding does not affect the mechanical properties of the corrosion-resistant steel bar. Welding can be used for corrosion-resistant steel bars because, after welding, the design requirements of the bearing capacity can be met.

Figure 1. Topography of welded steel bars: (a) before the tensile test and (b) after the tensile test

2.2 Mix proportion

An air-entraining agent and a polycarboxylic superplasticizer were used to adjust the air content of fresh concrete by approximately 3% to 5% and the slump of fresh concrete by approximately 180 mm to 220 mm, respectively. A solution-polymerized superabsorbent polymer (SAP) was used as an internal curing agent. The SAP was fed with water first before use, and the water absorbency was 30 g water/1 g SAP. The mixture proportion of concrete is listed in Table 4. The standard compressive strengths of concrete after curing for 3 d, 7 d, 28 d, and 56 d were tested, and the results were 41.6 MPa, 52.6 MPa, 61.5 MPa, and 68.9 MPa, respectively.

Table 4. Mix proportion of concrete (kg/m^3)

Cement	FA	GGBS	Sand	Granite	Water	Air entraining agent	Water reducing agent	SAP
250	75	145	730	1095	125	0.22	6	1

2.3 Experimental program

2.3.1 Preparation of concrete samples with cracks

Reinforced concrete specimens with 15 mm grooves on their surfaces were cast in a mould with a size of 100 mm ×100 mm × 300 mm. Before casting, the steel bars were pretreated by pickling and sanding. After removing 25 mm from the left and right ends, the wires were bonded to both ends, and epoxy resin was used for sealing to ensure that the exposed length of the steel bar was 250 mm. Then, five types of steel bars (LC, CR, and three welded steels) with a 10 mm diameter were set in concrete (the concrete cover was 25 mm thick).

Plastic flakes with 0.15 mm thicknesses were used to prepare transverse cracks perpendicular to the rebar, as shown in Figure 2. These plastic flakes were inserted into concrete samples during the initial setting stage and were pulled out before the final setting stage.

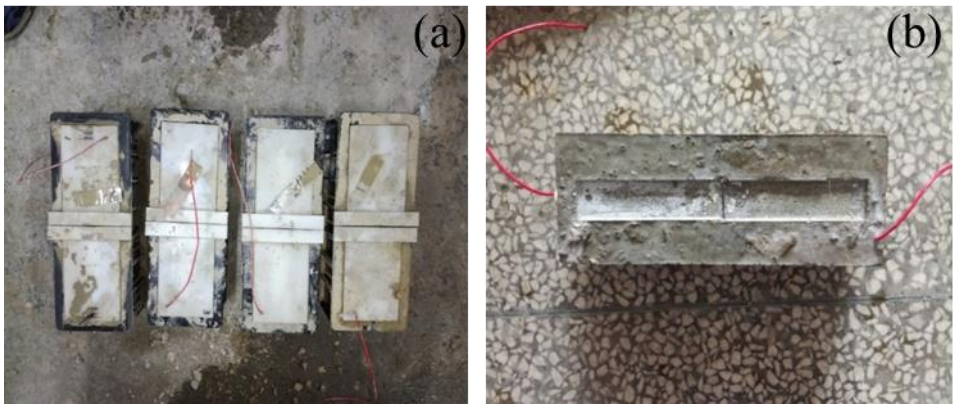

Figure 2. The casting of concrete specimens with cracks: (a) cast concrete and (b) after mould removal

2.3.2 Accelerated corrosion tests

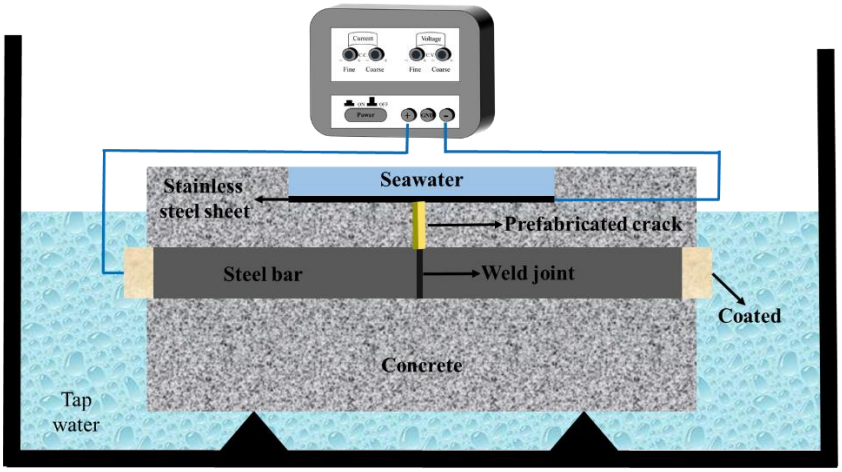

Figure 3. The schematic diagram of accelerated corrosion.

As shown in Figure 3, the reinforced concretes were used as a medium to accelerate corrosion under potentiostatic conditions that were kept constant at 30 V. The current was continuously tested every 1 ~ 2 h during the daytime and every 8 ~ 10 h at night. The entire duration of the accelerated corrosion test was 18 to 180 h according to different series. The reinforced concretes were immersed in tap water, and the groove on its surface was filled with seawater. The positive and negative poles of the DC power supply were severely connected to the steel bar in the concrete (anode) and auxiliary steel bar-a stainless steel rod (cathode). In addition, a digital camera was used to monitor the corrosion of reinforced concrete at any time.

2.3.3 EIS tests

As shown in Figure 4, in this study, the reinforced concretes were tested in Princeton Versa STAT 3 Series electrochemical workstations by a three-electrode system. The saturated calomel electrode (SCE), stainless steel bar, and steel bar in the concrete specimen were used as the reference electrode, counter electrode, and working electrode, respectively. To explain the corrosion process in detail, a qualitative analysis was performed, and a Nyquist diagram was obtained from the EIS test. ZSimpWin fitting software and the Stern-Geary formula were introduced to obtain future parameters.

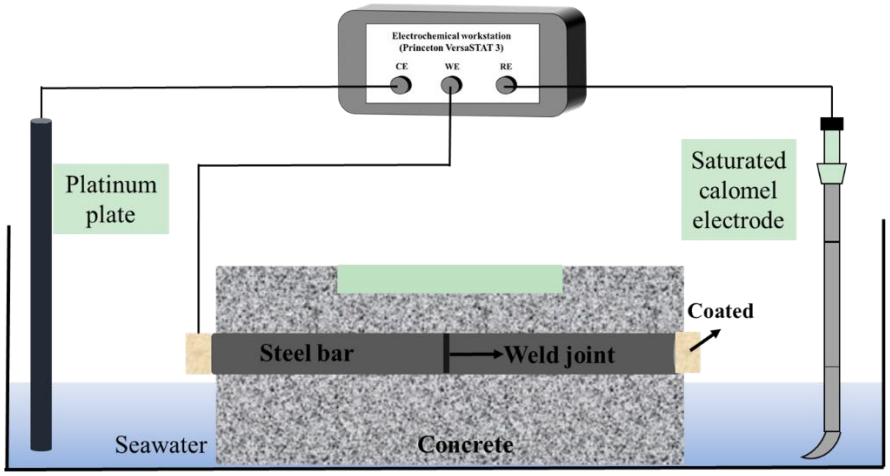

Figure 4. Schematic of testing corrosion using EIS

3. RESULTS AND DISCUSSION

3.1 Effect of welding on the corrosion behaviour of steel bars in concrete

3.1.1 Corrosion behaviour of welded and non-welded steel bars

Figure 5 shows the evaluation of the Nyquist and Bode plots of the welded and nonwelded steel bars in concrete. The diameter of the semicircle shown in the Nyquist plots can characterize the resistance on the surface of the steel bars. The low-frequency band principally controlled by the material

transfer process in the impedance spectrum reflects the corrosion of the steel bars in the concrete. When the slope of the low-frequency band curve rises, the steel bars have a large transfer resistance and are in a passivated state. At this time, the steel bars in the concrete have better corrosion resistance. A capacitive reactance arc appeared in the low-frequency band as the corrosion time increased. If the steel bars have a smaller capacitive arc radius, they will be more likely to corrode [34]. In the Bode phase plots, the greater the absolute value of the maximum phase angle is in the low-frequency region, the more stable the metal in the electrochemical system.

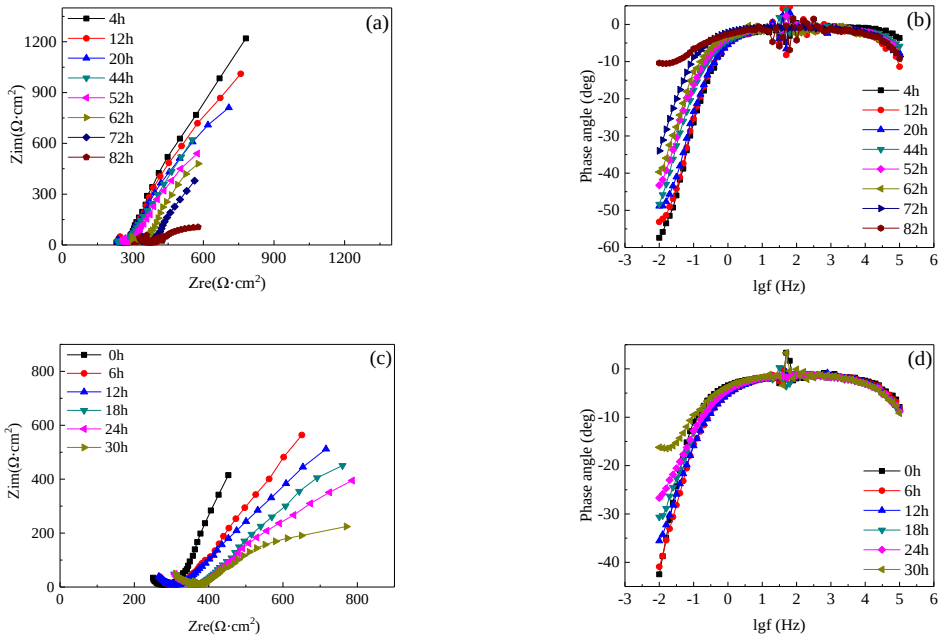

Figure 5. Nyquist and Bode plots of welded and nonwelded steel bars in concrete. (a) Nyquist plots of LC, (b) Bode plots of LC, (c) Nyquist plots of welded LC & LC, and (d) Bode plots of welded LC & LC

There is a high-frequency loop and a low-frequency loop in the Nyquist plot. The diameter of the capacitive loop shrank gradually with increasing corrosion time, and the corrosion times needed to produce obvious changes in the capacitive resistance arcs of the different types of steel bars were different. The topological structure of the Nyquist diagram has not undergone a qualitative change when the power was just turned on, and the low-frequency part exhibits an upward slope. This indicates that the impedance and capacitance of the passive film on the surface of the steel bar are very large, and the protective ability of the passive film is not undermined. The capacitive reactance arc in the Nyquist diagram gradually contracts significantly as the corrosion time increases. The topological structure of the low-frequency loop changes from a straight upward line to a flattened capacitive arc. The passive film on the surface of the steel bars in the concrete has undergone a qualitative change. Moreover, the impedance spectrum shows that the times corresponding to the obvious changes in the impedance spectra of welded and nonwelded steel bars are different. The times at which the capacitive arc is changed for the welded steel bars and nonwelded bars are 24 h and 72 h, respectively. It can be concluded that the

corrosion time of the steel bar is accelerated to 48 h by weld. Additionally, the absolute value of the maximum phase angle of welded steel bars is lower than that of nonwelded steel bars.

The obvious change in the capacitive resistance arc indicates that the steel bar is about to corrode, and its corrosion degree can be analysed quantitatively. AC impedance spectroscopy only qualitatively characterizes the corrosion of steel bars through a graphical topological structure, and it also needs to be fitted by ZsimpWin software to obtain corrosion parameters for auxiliary analysis [35]. The polarization resistance R_P of the steel bar was obtained by fitting. Then, R_P was introduced into the Stern-Geary formula, and the corrosion current density of the steel bar was calculated. The obtained Nyquist plots were fitted with equivalent circuits *R (R (Q (RQ)))* and *R(R (Q(R (QW)))* by ZsimpWin software, as shown in Figure 6. For the light corrosion stage, circuit *R (R (Q (RQ)))* is applied for fitting; when the corrosion is severe in the later stage, circuit *R(R (Q(R (QW)))* is applied for fitting.

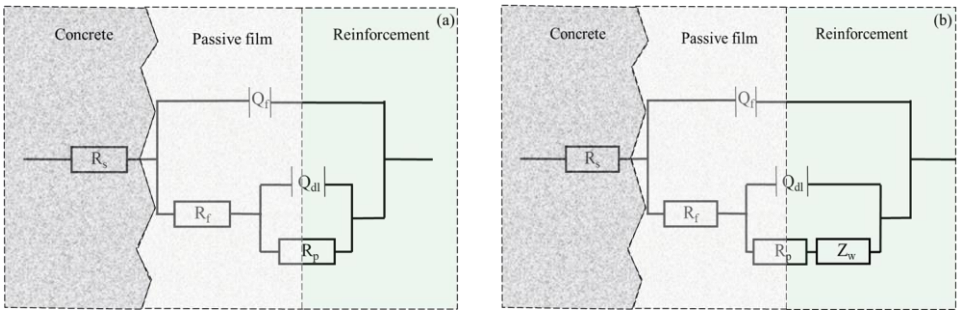

Figure 6. Equivalent circuits used for the simulation of EIS results. (a) R (R (Q (RQ))) (b) R(R (Q(R (QW))), where R_s is the resistance between the concrete and steel bar; Q_f is the capacitance; R_f is the passive film resistance of the steel bar; Q_{dl} is the double capacitance; R_P is the polarization resistance; and Z_w is the diffusion resistance.

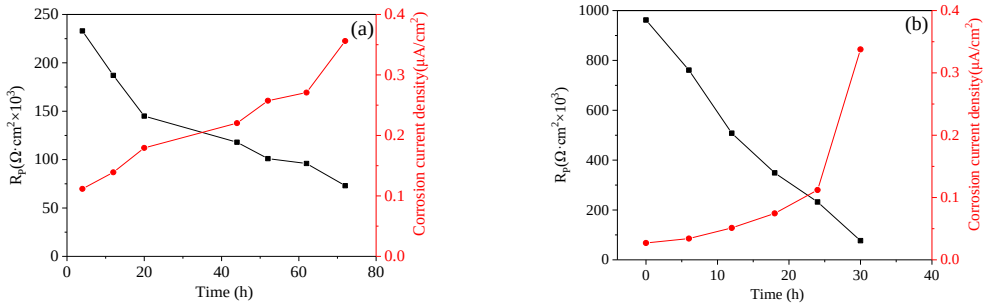

Figure 7. Calculated corrosion current density and R_P of welded steel bars and nonwelded bars in concrete: (a) nonwelded steel bar and (b) welded steel bar

The polarization resistance (R_P) was calculated by simulating equivalent-circuit models. Meanwhile, the instantaneous corrosion rate (i_{corr}) of the steel bar can be obtained from the polarization resistance (R_P) via the Stern-Geary equation shown in Eq. 1. The polarization resistance and instantaneous corrosion rate results are shown in Figure 7.

$$i_{corr} = \frac{B}{R_p} \qquad (1)$$

where B is a function of the Tafel slope. For steel bars in concrete, B values of 26 mV for the active state and 52 mV for the passive state have been proposed [36].

With increasing corrosion time, the current density of the two specimens increases with decreasing polarization resistance of the steel bar, as shown in Figure 7. However, the changing situations of the two types of steel bars and different periods are different. When the steel protective film is in a passivated state, the polarization resistance of the steel exhibits a small change, and its corrosion current density increases slowly. When the steel passive film is damaged and begins to rust, the polarization resistance and the corrosion current density of the steel bars change sharply. Figure 7 shows that after accelerating corrosion for 24 h, a large increase in the corrosion current density of the welded steel bar is observed. However, the corrosion current density of the nonwelded steel bar is still low. It can be concluded that welded steel bars are activated earlier than nonwelded bars. Similar to the report by Zhang et al. [37], ferrite presents a higher volume fraction and more easily suffers from corrosion attack than austenite in the welded zone of the as-welded metal.

3.1.2 Corrosion behaviour of welded steel bars of different weld types

Figure 8 shows the Nyquist and Bode plots of welded steel bars with different types in concrete. There are three types of welded steel bars: welded low-carbon steel and low-carbon steel (LC & LC), welded of corrosion-resistant steel and low-carbon steel (LC & CR), and welded corrosion-resistant steel and corrosion-resistant steel (CR & CR). The Nyquist plots show that the capacitive resistance arc of welded CR & CR exhibits the largest contraction change. Therefore, welding corrosion-resistant steel bars and corrosion-resistant steel bars, has the most significant effect on the corrosion behaviour of steel bars. In the Bode plots, the maximum phase angle of the three types of welded steel bars is between 40° and 50° before the beginning of energization. With increasing energization time, the phase angle gradually decreases and transfers to the high-frequency band, which indicates that the corrosion resistance of the steel bar gradually decreases. When the corrosion time was 6 h, the largest decrease in the phase angle appeared in the welded CR & CR samples.

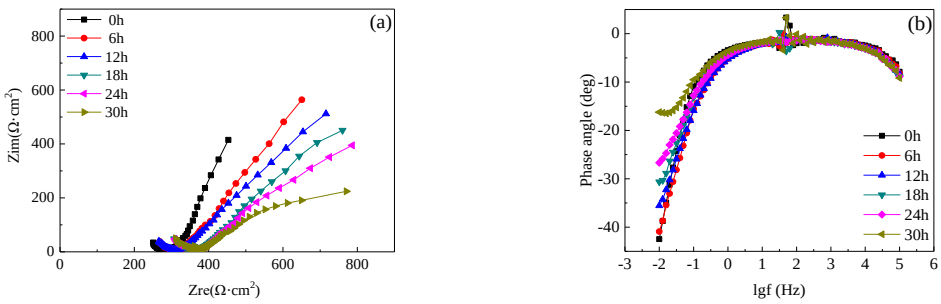

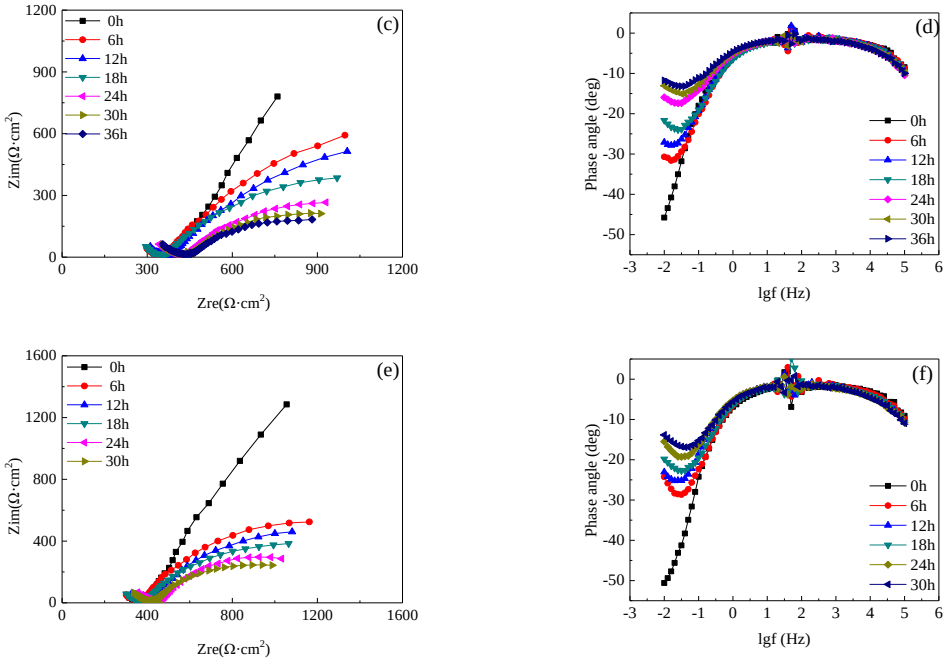

Figure 8. Nyquist and Bode plots of welded steel bars of different welding types. (a) Nyquist plots of welded LC & LC, (b) Bode plots of welded LC & LC, (c) Nyquist plots of welded LC & CR, (d) Bode plots of welded LC & CR, (e) Nyquist plots of welded CR & CR, and (f) Bode plots of welded CR & CR

The polarization resistance and instantaneous corrosion rate results are shown in Figure 9. The order of the corrosion start time is CR & CR > LC & CR > LC & LC, and the activation time of welded corrosion-resistant steel bars is approximately 18 h shorter than that of welded ordinary steel bars. This illustrates that the influence of welding on corrosion-resistant steel is greater than that on ordinary steel. The main reason for this is that the corrosion-resistant steel bars contain other alloying elements. Phase transformation occurs at a high temperature during welding, which makes it more prone to corrosion [38].

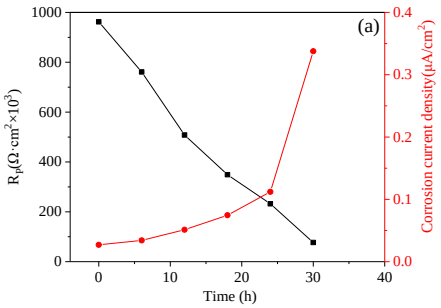

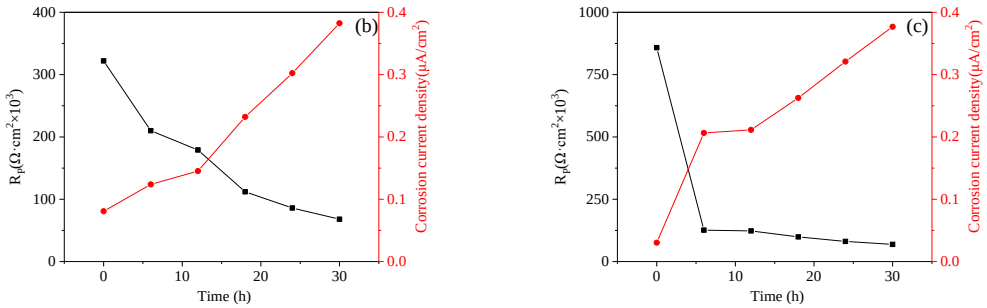

Figure 9. Calculated corrosion current density and R_P of welded steel bars of different weld types: (a) welded LC & LC, (b) welded LC & CR, and (c) welded CR & CR

3.2 Effect of cracks on the corrosion behaviour of steel bars in concrete

3.2.1 Corrosion behaviour of nonwelded steel bars in concrete with and without cracks

(1) Macroscopic phenomenon and corrosion current evolution

Figure 10 shows that in the early stage of steel corrosion, red-brown rust overflowed from the prefabricated cracks. The prefabricated cracks became wider due to tension during the overflow of the rust. In the later stage of steel corrosion, steel swelling caused the concrete protective layer to crack. When accelerated corrosion was carried out, rust gradually accumulated, and the prefabricated cracks on the concrete surface continued to widen and expand. Splitting the completely rusted test block, as shown in Figure 10 (c), shows that the electrically accelerated rust is uneven. In addition, the steel bars on the side close to the site of seawater infiltration are very severely corroded, while the steel bars on the other side exhibit almost no corrosion.

Figure 10. Crack propagation of concrete (a) before rust formation and (b) after rust formation. (c) Corrosion distribution

The corrosion of two types of reinforced concrete specimens after 28 days of standard curing was accelerated until the current changed suddenly, and then, energization was stopped. An instrument was used to record the current change with respect to the power-on time, as shown in Figure 11. In the early stage of electrification, the currents of the two types of reinforced concrete specimens tend to be stable. With increasing accelerating time, the currents slowly decrease. After accelerating corrosion for a period, the currents tend to be stable after a large sudden change. At this time, the concrete surface began to overflow with rust, which expanded the concrete specimen along the prefabricated cracks. When a sudden current change occurs, cracks will appear on the surface of the concrete, and the specimen will be completely cracked. According to the point at which the current suddenly changes, the cracking times of low-carbon steel and corrosion-resistant reinforced concrete specimens are 113 h and 154 h, respectively. The energization time of corrosion-resistant reinforced concrete is approximately 40 h longer than that of low-carbon steel. The main reason for this is that the corrosion-resistant steel bars have good corrosion resistance and are not easily corroded. Rust formation produced is slow, and the concrete specimens crack late in the process.

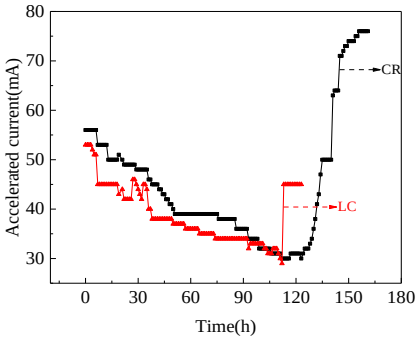

Figure 11. The change in accelerated current with time

(2) The Nyquist and Bode plots

Figure 12 shows the Nyquist and Bode plots of nonwelded steel bars in concrete with and without cracks. As the energization time increases, the impedance curve of the continuously reinforced concrete shrinks, which leads to a continuous decrease in the capacitive arc radius. However, the time at which the capacitive reactance arc changes significantly is different. Under the same electrical acceleration conditions, the capacitive arc of the nonwelded steel bars in concrete with cracks exhibits obvious shrinkage changes when electricity was applied for 6 h. The capacitive resistance arc of the nonwelded steel bars in concrete without cracks is still a straight line, and there is no obvious shrinkage change until 72 h after electrification. This illustrates that the cracks advanced the corrosion time of the nonwelded steel bars in concrete by more than 60 h. In the Bode plots, the phase angle of the nonwelded steel bars decreases more significantly with increasing energization time, indicating that the cracks have a greater impact on the nonwelded steel bars.

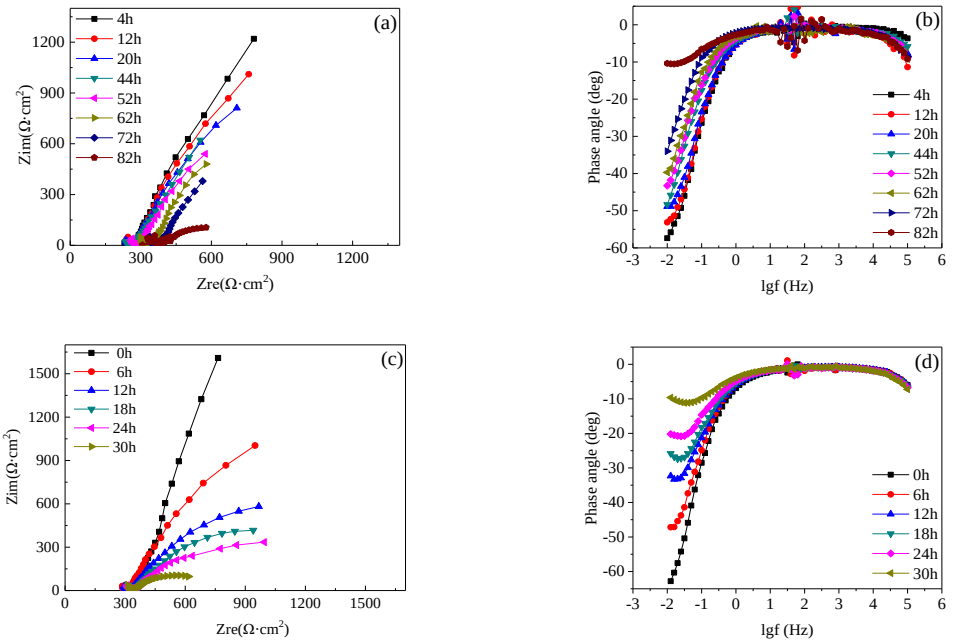

Figure 12. Nyquist and Bode plots of nonwelded steel bars in concrete with and without cracks. (a) Nyquist plots of the concrete without cracks. (b) Bode plots of the concrete without cracks. (c) Nyquist plots of the concrete with cracks. (d) Bode plots of the concrete with cracks

Figure 13 shows the calculated corrosion current density and R_P of nonwelded steel bars in concrete. As the energization time increases, the current density of the two specimens shows an increasing trend, and the polarization resistance of the steel bar decreases. When $i_{coor} < 0.1$ μA/cm^2, the steel bar is in a passivated state, and when $0.2 \leq i_{coor} < 0.5$ μA/cm^2, the steel bar is in a low corrosion rate state. The activation of nonwelded steel bars in concrete with cracks begins at an early stage. The activation of nonwelded steel bars in concrete is advanced by approximately 14 h due to cracks. As reported by Lopez-Calvo [39], cracks are found to be an influencing factor promoting the corrosion of steel in concrete.

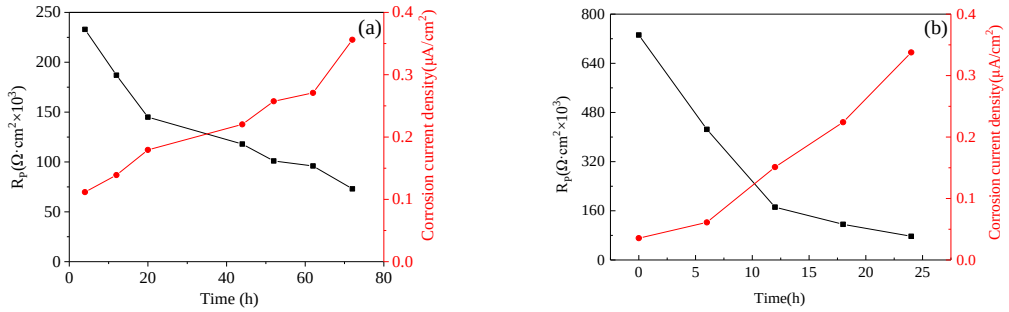

Figure 13. Calculated corrosion current density and R_P of nonwelded steel bars in concrete: (a) concrete without cracks and (b) concrete with cracks

3.2.2 Corrosion behaviour of welded steel bars in concrete with and without cracks

The change in the corrosion current of the welded steel bars in concrete was monitored in real-time through a camera, as shown in Figure 14. The initial current value of the welded CR & CR samples was relatively low. From the point at which the current suddenly changes, it can be concluded that the cracking time of the welded steel bars of LC & LC, LC & LC-crack, LC & CR, LC & CR-crack, CR & CR, and CR & CR-crack in concrete is 50 h, 22 h, 36.5 h, 12 h, 50.5 h, and 15.5 h, respectively. The order of the total power-on time is CR & CR > LC & CR > LC & LC > LC & LC-crack > CR & CR-crack > LC & CR-crack. In addition, the order of the accelerated current magnitude during power-on is: LC & LC-crack > LC & CR-crack > LC & LC > LC & CR > CR & CR-crack > CR & CR. In summary, it can be concluded that the LC & CR-crack samples have the fastest corrosion rate and the shortest cracking time. The main reason for this is that the progress of galvanic corrosion has been promoted by cracks for LC & CR welded steel bars. As reported by Pantelis [40], galvanic corrosion appears as the preferential corrosion type on HAZ, owing to the different corrosion susceptibilities of the distinct weldment microstructures. Additionally, the CR & CR sample has the slowest corrosion rate and the longest cracking time. The cracking time of welded steel bars in concrete is advanced by approximately 30 h due to cracks.

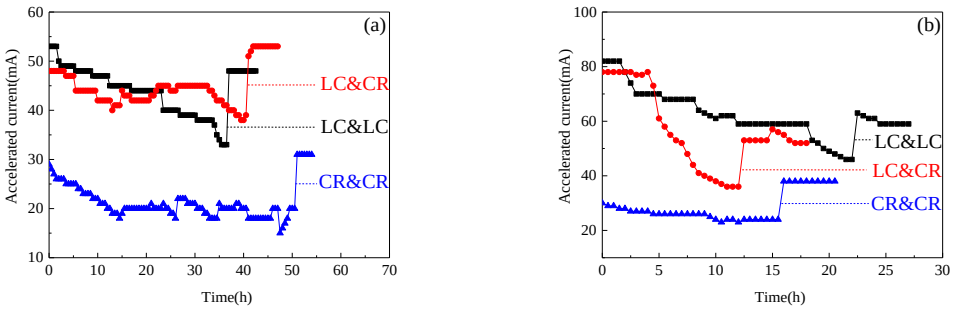

Figure 14. The change in the accelerated current with time: (a) concrete without cracks and (b) concrete with cracks

Figure 15 shows the Nyquist and Bode plots of welded steel bars in concrete with and without cracks. The curve position of the welded steel bars in concrete with cracks is significantly shifted to the left relative to that of the concrete without cracks. This indicates that under the conditions of accelerated corrosion, the welded steel bars in concrete with cracks corrode significantly faster than those in concrete without cracks. The slope of welded LC & LC curve changes significantly when the acceleration time is 15 h.

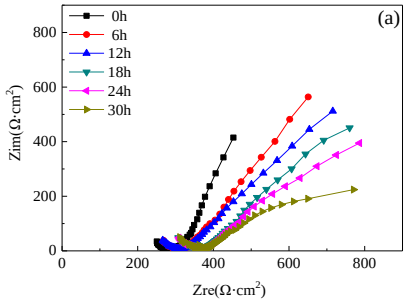
(a)
0h
6h
12h
18h
24h
30h
Zim(Ω·cm²)
Zre(Ω·cm²)

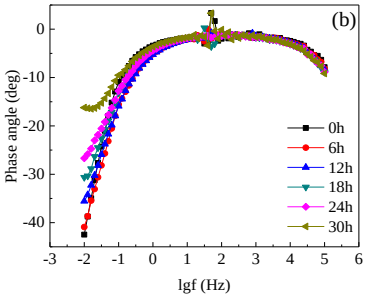
(b)
0h
6h
12h
18h
24h
30h
Phase angle (deg)
lgf (Hz)

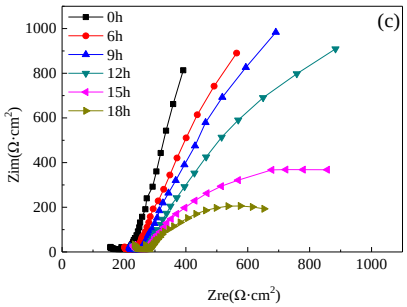
(c)
0h
6h
9h
12h
15h
18h
Zim(Ω·cm²)
Zre(Ω·cm²)

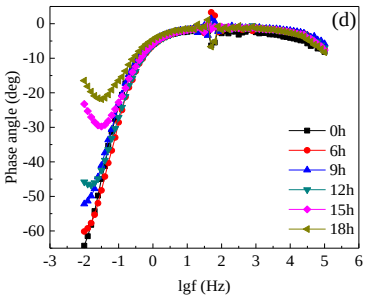
(d)
0h
6h
9h
12h
15h
18h
Phase angle (deg)
lgf (Hz)

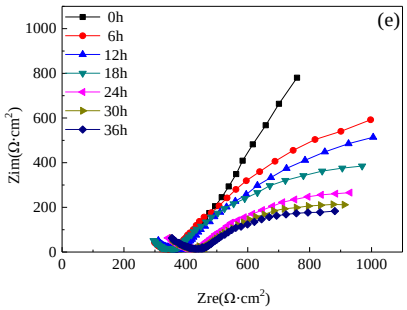
(e)
0h
6h
12h
18h
24h
30h
36h
Zim(Ω·cm²)
Zre(Ω·cm²)

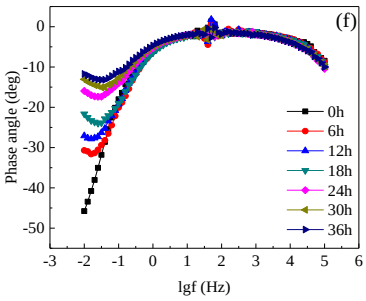
(f)
0h
6h
12h
18h
24h
30h
36h
Phase angle (deg)
lgf (Hz)

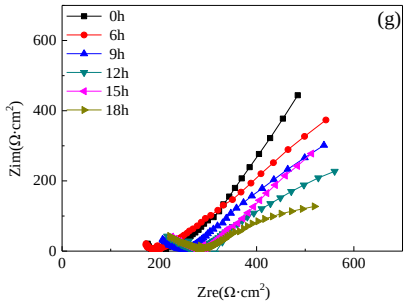
(g)
0h
6h
9h
12h
15h
18h
Zim(Ω·cm²)
Zre(Ω·cm²)

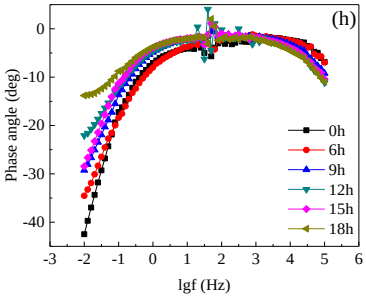
(h)
0h
6h
9h
12h
15h
18h
Phase angle (deg)
lgf (Hz)

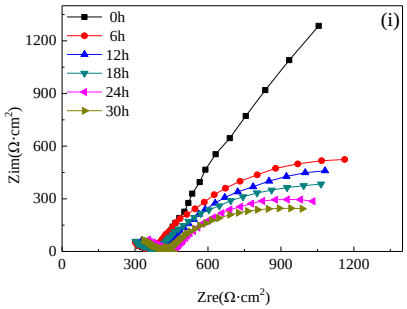
(i)
0h
6h
12h
18h
24h
30h
Zim(Ω·cm²)
Zre(Ω·cm²)

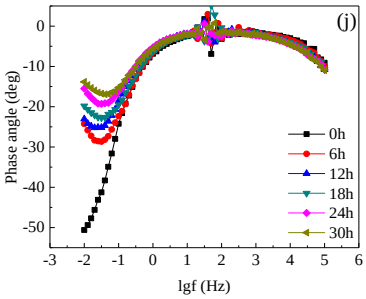
(j)
0h
6h
12h
18h
24h
30h
Phase angle (deg)
lgf (Hz)

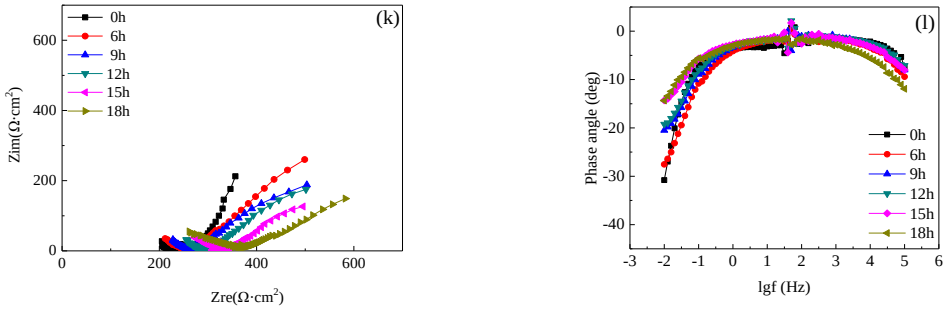

Figure 15. Nyquist and Bode plots of welded steel bars in concrete with and without cracks: (a) Nyquist plots of LC & LC, (b) Bode plots of LC & LC, (c) Nyquist plots of LC & LC-crack, (d) Bode plots of LC & LC-crack, (e) Nyquist plots of LC & CR, (f) Bode plots of LC & CR, (g) Nyquist plots of LC & CR-crack, (h) Bode plots of LC & CR-crack, (i) Nyquist plots of CR & CR, (j) Bode plots of CR & CR, (k) Nyquist plots of CR & CR-crack, and (l) Bode plots of CR & CR-crack

However, for the other types, the same phenomenon is not found. In addition, the Bode plots show that as the energization time increases, the phase angle of welded steel bars with cracks decreases more significantly. Moreover, the absolute value of the initial phase angle of CR & CR-crack is the smallest, indicating that cracks have the greatest impact on the welding of corrosion-resistant steel bars.

Figure 16 shows the polarization resistance and corrosion current density of the welded steel bars in concrete with and without cracks. The acceleration time of welded steel bars in concrete without cracks is approximately twice as long as that in concrete with cracks. For the welded LC & LC sample, the corrosion current density exceeded 0.5 μA/cm^2 when the acceleration time was 18 h. This illustrates that for the welded LC & LC sample, the corrosion current density was increased by cracks. In addition, the activation of welded steel bars in concrete is advanced by approximately 15 h due to cracks.

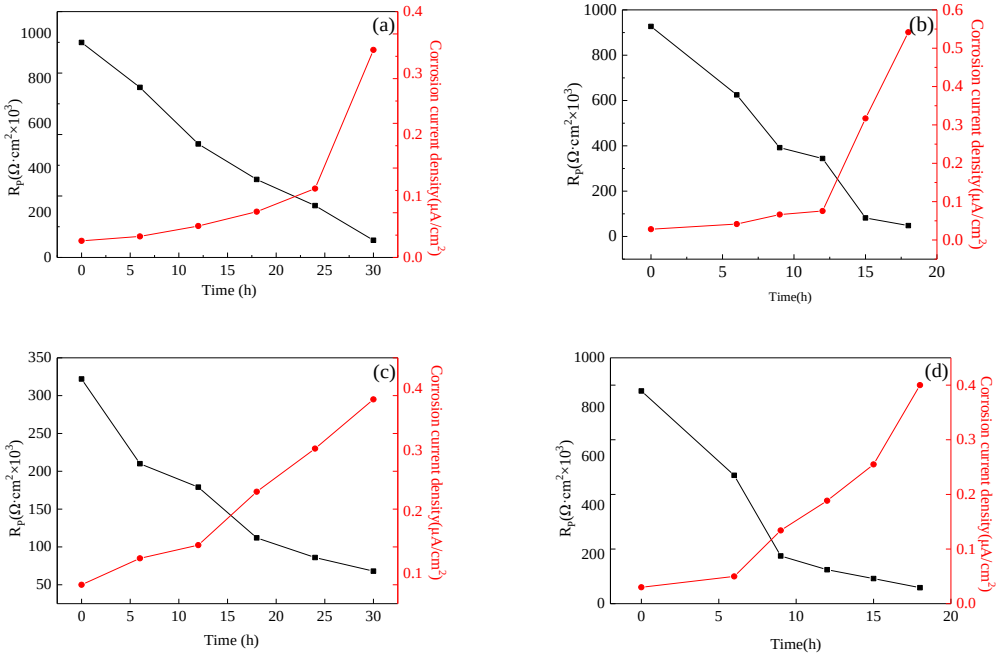

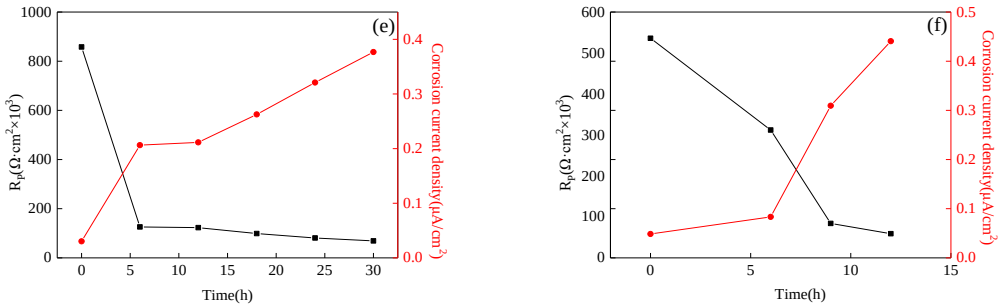

Figure 16. Calculated corrosion current density and R_P of the welded steel bars in concrete with and without cracks: (a) LC & LC (b), LC & LC-crack, (c) LC & CR, (d) LC & CR-crack, (e) CR & CR, and (f) CR & CR-crack

4. CONCLUSIONS

In this paper, concrete with and without cracks is prepared to study the corrosion behaviour in concrete reinforced with welded steel bars and that in concrete not welded through electrochemical technology. Based on the experimental corrosion results, the following conclusions are drawn.

(1) The depassivation time of the steel bars is shortened by 48 h by welding, illustrating that the steel bars are more prone to corrosion due to welding. For the welded CR & CR sample, that influence is most significant. The depassivation time of welded corrosion-resistant steel bars is approximately 18 h shorter than that of welded ordinary steel bars.

(2) The corrosion time and depassivation time of the nonwelded steel bars in concrete were advanced by approximately 60 h and 14 h, respectively, due to cracks. For the welded steel bars in concrete, the depassivation time was advanced by approximately 15 h due to cracks. Because the progress of galvanic corrosion was promoted by cracks, the influence is most significant for the welded LC & CR steel bars. The corrosion current density of welded LC & LC sample was increased by cracks.

ACKNOWLEDGEMENTS
This work is a part of a series of projects financially supported by the National Natural Science Foundation of China (NSFC), Grant No. U1806225 and 52078259, 5191102012, and the MOUNT TAI Scholar of Shandong Province (ts20190942). Besides, this work is also supported by National 111 project. All these supports are gratefully appreciated.

References

1. Z.Q. Jin, H.L. Chang, F.Y. Du, T.J. Zhao, Y.D. Jiang and Y.F. Chen, *Corros. Sci.*, 171 (2020) 108714.
2. Z.Q. Jin, X. Z, T.J. Zhao and J.Q. Li, *Constr. Build. Mater.*, 177 (2018) 170.
3. F.L. Qu, W.G. Li, W.K. Dong, Vivian.W.Y. Tam and T. Yu, *J. Build. Eng.*, 35 (2021) 102074.
4. C.S. Xiong, W.H. Li, Z.Q. Jin, X. Gao, W. Wang, H.W. Tian, P. Han, L.Y. Song and L.H. Jiang, *Corros. Sci.*, 139 (2018) 275.
5. Z.Q. Jin, D.S. Hou and T.J. Zhao, *Constr. Build. Mater.*, 173 (2018) 149.
6. I. Odnevall Wallinder, J.S. Lu, S. Bertling and C. Leygraf, *Corros. Sci.*, 44 (2002) 2303.
7. D. Hamm, K. Ogle, C.O.A. Olsson, S. Weber and D. Landolt, *Corros. Sci.*, 44 (2002) 1443.

8. M. Criado, D.M. Bastidas, S. Fajardo, A. Fernández-Jiménez and J.M. Bastidas, *Cem. Concr. Compos.*, 33 (2011) 644.
9. M. Liu, X.Q. Cheng, X.G. Li, Z. Jin and H.X. Liu, *Constr. Build. Mater.*, 93 (2015) 884.
10. M. F. Hurley and J. R. Scully, *Corr05.*, 62 (2006) 892.
11. L. Freire, M.J. Carmezim, M.G.S. Ferreira and M.F. Montemor, *Electrochim. Acta*, 55 (2010) 6174.
12. M. Serdar, L.V. Žulj and D. Bjegović, *Corros. Sci.*, 69 (2013) 149.
13. C. Garcia, F. Martin, P. de Tiedra, Y. Blanco and M. Lopez, *Corros. Sci.*, 50 (2008) 1184.
14. C. Garcia, M.P. de Tiedra, Y. Blanco, O. Martin and F. Martin, *Corros. Sci.*, 50 (2008) 2390.
15. M. Dadfar, M.H. Fathi, F. Karimzadeh, M.R. Dadfar and A. Saatchi, *Mater. Lett.*, 61 (2007) 2343.
16. H. Kokawa, M. Shimada, M. Michiuchi, Z.J. Wang and Y.S. Sato, *Acta Mater.*, 55 (2007) 5401.
17. S. Tokita, K. Kadoi, S. Aoki and H. Inoue, *Corros. Sci.*, 175 (2020) 108867.
18. M.A. Derakhshi, J. Kangazian and M. Shamanian, *Vac.*, 161 (2019) 371.
19. R.K. Gupta and N. Birbilis, *Corros. Sci.*, 92 (2015) 1.
20. C.M. Lin, H.L. Tsai, C.D. Cheng and C. Yang, *Eng. Fail. Anal.*, 21 (2012) 9.
21. S.W. Tang, Y. Yao, C. Andrade and Z.J. Li, *Cem. Concr. Res.*, 78 (2015) 143.
22. A. Gnanarathinam, D. Palanisamy, N. Manikandan, A. Devaraju and D. Arulkirubakaran, *Mater. Today:. Proc.*, (2020).
23. K.F. Li and L. Li, *Cem. Concr. Res.*, 124 (2019) 105811.
24. Z.Q. Jin, X. Zhao, T.J. Zhao and L. Yang, *Constr. Build. Mater.*, 113 (2016) 805.
25. K.J. Wang, D.C. Jansen, S.P. Shah and A.F. Karr, *Cem. Concr. Res.*, 27 (1997) 381.
26. M. Ismail, A. Toumi, R. François and R. Gagné, *Cem. Concr. Res.*, 38 (2008) 1106.
27. S.Y. Jang, B.S. Kim and B.H. Oh, *Cem. Concr. Res.*, 41 (2011) 9.
28. W.J. Zhu, R. François, C.P. Zhang and D.L. Zhang, *Cem. Concr. Res.*, 103 (2018) 66.
29. C. Cao, M.M.S. Cheung and B.Y.B. Chan, *Corros. Sci.*, 69 (2013) 97.
30. F. Xu, Y.F. Xiao, S.G. Wang, W.W. Li, W.Q. Liu and D.S. Du, *Constr. Build. Mater.*, 180 (2018) 55.
31. F.Y. Du, Z.Q. Jin, W. She, C.S. Xiong, G.Y. Feng and J.F. Fan, *Constr. Build. Mater.*, 263 (2020) 120099.
32. Y.S. Ji, Y.J. Hu, L.L. Zhang and Z.Z. Bao, *Cem. Concr. Res.*, 69 (2016) 28.
33. Z.Y. Ai, J.Y. Jiang, W. Sun, D. Song, H. Ma, J.C. Zhang and D.Q. Wang, *Appl. Surf. Sci.*, 389 (2016).
34. D.V. Ribeiro and J.C.C. Abrantes, *Constr. Build. Mater.*, 111 (2016) 98.
35. J.J. Shi, J. Ming, W. Sun and Y.M. Zhang, *Constr. Build. Mater.*, 149 (2017) 315.
36. C. Andrade and C. Alonso, *Constr. Build. Mater.*, 10 (1996) 315.
37. Z.Y. Zhang, Z.Y. Wang, Y.M. Jiang, H. Tan, D. Han, Y.J. Guo and J. Li, *Corros. Sci.*, 62 (2012) 42.
38. Z.Q. Zhang, H.Y. Jing, L.Y. Xu, Y.D. Han, L. Zhao and X.Q. Lv, *Corros. Sci.*, 141 (2018) 30.
39. H.Z. Lopez-Calvo, P. Montes-García, V.G. Jiménez-Quero, H. Gómez-Barranco, T.W. Bremner and M.D.A. Thomas, *Cem. Concr. Compos.*, 88 (2018) 200.
40. D.I. Pantelis and T.E. Tsiourva, *Trends in Oil and Gas Corrosion Research and Technologies*, Woodhead Publishing, (2017) Boston, America.